

1 Observations of low-latitude plasma density 2 enhancements and their associated plasma drifts

J. H. Klenzing,¹ D. E. Rowland,¹ R. F. Pfaff,¹ G. Le,¹ H. Freudenreich,¹ R. A. Haaser,² A. G. Burrell,² R. A. Stoneback,² W. R. Coley,² and R. A. Heelis²

J. H. Klenzing, NASA Postdoctoral Program Fellow, Space Weather Laboratory, Code 674, Goddard Space Flight Center, Greenbelt, MD 20771, USA. (jeffrey.klenzing@nasa.gov)

¹Space Weather Laboratory / Code 674,
Goddard Space Flight Center, Greenbelt,
Maryland, USA

²Center for Space Sciences, The
University of Texas at Dallas, MS WT15,
Richardson, Texas, USA.

3 **Abstract.** Plasma density structures are frequently encountered in the
4 nighttime low-latitude ionosphere by probes on the Communication/Navigation
5 Outage Forecasting System (C/NOFS) satellite. Of particular interest to us
6 here are plasma density enhancements, which are typically observed $\pm 15^\circ$
7 away from the magnetic equator. The low inclination of the C/NOFS satel-
8 lite offers an unprecedented opportunity to examine these structures and their
9 associated electric fields and plasma velocities, including their field-aligned
10 components, along an east-west trajectory. Among other observations, the
11 data reveal a clear asymmetry in the velocity structure within and around
12 these density enhancements. Previous observations have shown that the peak
13 change in drift velocity associated with a density enhancement occurs simul-
14 taneously both perpendicular and parallel to the magnetic field, while the
15 results in this paper show that the peak change in parallel flow typically oc-
16 curs 25-100 km to the east of the peak perpendicular flow. We discuss this
17 and other aspects of the observations in relation to the characteristics of the
18 plasma depletions formed near the magnetic equator detected by the same
19 probes on the C/NOFS satellite and to previous observations and theories.

1. Introduction

20 Ionospheric scintillation refers to the scattering of radio waves interacting with an ir-
21 regular ion density layer in the upper atmosphere and is an important concern for the
22 successful operation of GPS, radar, and other communication signals. For historical rea-
23 sons, various types of equatorial plasma density irregularities have been classified under
24 the generic name Equatorial Spread-F (ESF) due to their common effect on radar echoes
25 in the F-region Ionosphere [*Kelley, 2009*]. One of the better understood irregularities
26 associated with ESF is the plasma density depletion, also referred to as a plasma “bub-
27 ble,” which is formed by a Rayleigh-Taylor instability acting of the bottomside of the
28 F-layer [*e.g., Fejer and Kelley 1980*]. ESF plasma depletions appear as elongated plumes
29 of relatively low density in radar data [*Woodman and La Hoz, 1976*] and as curved region
30 of reduced optical emission from space-borne imagers [*Kil et al., 2009*]. More recently,
31 plasma density enhancements, sometimes referred to as “blobs,” have been observed in
32 the vicinity in plasma depletions, leading to much discussion about the potential relation
33 between these two density structures.

34 Plasma enhancements were first reported from ion density and temperature data from
35 the Hinotori satellite [*Oya et al., 1986*]. They were found to occur beyond the edge of
36 the region of occurrence for bubbles, typically about 15 degrees away from the magnetic
37 equator in either hemisphere. *Watanabe and Oya [1986]* examined the statistics of oc-
38 currence and found that enhancements favor the winter hemisphere, typically occur after
39 midnight, and have a strong longitudinal variation pattern that varies as a function of
40 season. Based on a statistical analysis of enhancements and depletions encountered by

41 Hinotori, they concluded that the two phenomena must have different physical drivers,
42 with the depletions caused by $\mathbf{E}\times\mathbf{B}$ uplift and the enhancements caused by meridional
43 wind instabilities.

44 However, a number of recent observations have suggested a stronger link between the
45 evolution of bubbles and blobs. Observations from satellites [*Le et al.*, 2003], all-sky im-
46 agers [*Pimenta et al.*, 2007; *Martinis et al.*, 2009], radar [*Yokoyama et al.*, 2007], and
47 GPS TEC measurements [*Dashora and Pandey*, 2005] have shown density enhancements
48 forming simultaneously near depletions. *Yokoyama et al.* [2007] shows depletions and en-
49 hancements forming along the same flux tube using data from ROCSAT-1 and Equatorial
50 Atmosphere Radar. Density enhancements were also found along the same field lines as
51 ESF airglow depletions [*Martinis et al.*, 2009]. Statistical studies with satellite data from
52 KOMPSAT-1 and DMSP F15 have shown that the depletions and enhancements show
53 similar seasonal and longitudinal variations (with several exceptions) [*Park et al.*, 2008a].

54 *Le et al.* [2003] proposes a mechanism to link the two phenomena. Polarization electric
55 fields formed inside the depleted flux tubes are mapped down the magnetic field lines past
56 the region of depletion. These eastward polarization fields result in an upward $\mathbf{E}\times\mathbf{B}$ drift
57 that transports local plasma upward to just above the depleted flux tube, resulting in a
58 plasma density enhancement. This is supported by the similarity of the spectral properties
59 of density fluctuations inside the enhancements and depletions [*Le et al.* 2003] and by the
60 increase in the relative concentration of O^+ to H^+ inside the enhancement [*Yokoyama et*
61 *al.*, 2007]. Recent simulation work using the SAMI3 model shows that regions of enhanced
62 plasma density can form around spread F depletion plumes [*Krall et al.*, 2010].

63 The following work discusses recent observations of plasma density enhancements from
64 the C/NOFS satellite and their associated velocity and composition structures during a
65 period of very low solar flux. Both plasma density depletions and enhancements were
66 frequently encountered by the C/NOFS satellite during the first two years of operation
67 [Haaser et al., 2010]. While density enhancements have been observed on a number
68 of satellites including STSAT-1, CHAMP, and KOMPSAT-1 [Park et al., 2003, 2008b],
69 most of these satellites were only capable of measuring density and temperature. With
70 the exception of ROCSAT-1 observations and SAMI3 simulations, there has been little
71 discussion of the ion drifts inside and around the density enhancements. The plasma drifts
72 associated with density enhancements observed by C/NOFS will be compared the drifts
73 associated with density depletions.

2. Measurements

74 The Communication/Navigation Outage Forecast System (C/NOFS) satellite is part of
75 an Air Force mission to locate, understand, and predict equatorial ionospheric scintillation
76 using satellite measurements, complementary ground-based observations, and physics-
77 based models [de La Beaujardière et al., 2004]. The C/NOFS satellite was launched in
78 April 2008 into a 13° inclination orbit with perigee near 400 km and apogee near 860
79 km. C/NOFS consists of multiple instrument suites designed to study the ion and neutral
80 populations and their effect on the propagation of communication signals. This study will
81 focus on data from the Vector Electric Field Instrument (VEFI), provided by Goddard
82 Space Flight Center, and the Ion Velocity Meter (IVM), provided by the University of
83 Texas at Dallas.

84 VEFI consists of multiple sensors, including three electric field double probe booms, a
85 lightning detector, and a 3-axis flux-gate magnetometer [Pfaff *et al.*, 2010]. Of interest to
86 this study are the electric field probes and the magnetometer, which are used to provide
87 the $\mathbf{E} \times \mathbf{B}$ drifts perpendicular to the magnetic field. The two perpendicular directions
88 are defined as the meridional direction (positive outward in the plane of the magnetic
89 meridian) and the zonal direction (positive eastward perpendicular to the meridian plane).
90 The $\mathbf{E} \times \mathbf{B}$ drifts are averaged to one sample per second.

91 IVM, part of the Coupled Ion-Neutral Dynamics Investigation (CINDI) Mission of Op-
92 portunity on C/NOFS, consists of two sub-instruments: the retarding potential analyzer
93 (RPA) and the ion drift meter (IDM). These two instruments provide 3D ion drifts as well
94 as density, composition, and temperature information for the ion population [Heelis and
95 Hanson, 1998]. The measured velocities are rotated into the field-aligned reference frame
96 using the VEFI magnetometer measurements, providing the drift component parallel to
97 the magnetic field. The meridional component from the IVM is also compared to that
98 from VEFI. Unfortunately, the drift component from the RPA is not optimized due to the
99 low ion flux during this exceptionally deep solar minimum, so the zonal component from
100 the IVM (as well as the parallel and meridional components where the RPA contribution
101 is significant) will be neglected for the purpose of this study.

102 The C/NOFS data presented in this paper (Figures 1–6) are arranged into four panels
103 per figure, each containing 5–10 minutes of data. Panel (a) shows the density (N) plotted
104 on a log scale, with the total density plotted in black and the O^+ density plotted in blue.
105 The remainder of the density consists of light ions (H^+ and He^+). Panel (b) shows the
106 parallel drift (v_{\parallel}) derived from IVM; it is defined as positive northward. Panel (c) shows

107 the meridional $\mathbf{E} \times \mathbf{B}$ drift ($v_{\perp m}$) derived from both IVM (green) and VEFI (purple), and
 108 panel (d) shows the zonal $\mathbf{E} \times \mathbf{B}$ drift ($v_{\perp z}$) from VEFI. The important features are marked
 109 by a vertical orange line that corresponds to the peak change in density as determined by
 110 a quadratic fit to the density perturbation. All data is plotted as a function of UT, with
 111 the corresponding solar local time (SLT), altitude, magnetic dip angle, and geographic
 112 location listed on the x-axis.

3. Observation of Density Depletions

113 Figures 1 and 2 are examples of plasma density depletions observed by C/NOFS. Note
 114 that the depletions shown here are relatively weak (*i.e.*, density is reduced by less than
 115 one order of magnitude) compared to other recent studies [*e.g.*, *de La Beaujardière et al.*,
 116 2009] due to the difficulty in calculating accurate three-dimensional ion drifts inside the
 117 deep depletions (where density is reduced by several orders of magnitude). These “weak”
 118 depletions are similar to the upper regions of a depleted plasma shell as shown in the
 119 simulations of *Aveiro and Hysell* [2010]. The two figures show that:

120 1. The peak change in density occurs nearly simultaneously (*i.e.*, at the same longitude)
 121 with the peak change in velocity. This is similar to the ROCSAT observations of plasma
 122 depletions in the equatorial ionosphere [*Le et al.*, 2003].

123 2. A poleward change in drift is associated with most of the observed bubbles. Figure 1
 124 shows several depletions south of the dip equator. The depletions correspond to a negative
 125 (southward) change in v_{\parallel} . Depletions observed north of the dip equator (Figure 2) have
 126 a corresponding positive (northward) change in v_{\parallel} . Depending on the relative strengths of
 127 the irregularity and the background drift, the direction of parallel flow may or may not
 128 change.

129 3. The $\mathbf{E} \times \mathbf{B}$ perturbation drifts within the depletions are typically upward (meridional)
130 and westward (zonal), which correspond to a polarization electric field pointing up and
131 east. This corresponds to the fields expected in a westward-tilted plasma bubble [*Huang*
132 *et al.*, 2010]. There are several events where the zonal drift is noisy, and the relative
133 change associated with the bubble is unclear.

4. Observations of Density Enhancements

134 Figures 3-6 are examples of density enhancements observed by the C/NOFS satellite,
135 with the associated 3D ion drifts relative to the magnetic field. A vertical line marks a
136 local density increase $\geq 50\%$ above the background density. Plasma density enhancements
137 are observed during solstice and equinox in both magnetic hemispheres. Figures 3-5 show
138 density enhancements near the June solstice of 2009, with orbit tracks in the southern
139 (winter) magnetic hemisphere (Figure 3), in the northern (summer) magnetic hemisphere
140 (Figure 4), and near the magnetic dip equator (Figure 5). Figure 6 shows an event in the
141 southern hemisphere near the September equinox. All four plots show similar features, as
142 outlined below:

143 1. The enhancements show an increase in relative O^+ concentration, displacing lighter
144 ions. This indicates that plasma is being transported from regions with a lower apex
145 height. This is consistent with previous observations [*Yokoyama et al.*, 2007].

146 2. A poleward change in ion drift parallel to \mathbf{B} is associated with most of the observed
147 enhancements. Figure 3 shows several examples of enhancements in the southern magnetic
148 hemisphere; Figure 4 shows a series of events in the northern magnetic hemisphere. Note
149 that both events are near the June solstice; consequently, the background parallel drift is

150 toward the southern (winter) pole. Of the nine events in these two plots, seven show a
151 strong poleward shift in the parallel ion drift associated with the enhancement.

152 3. The peak change in $\mathbf{E} \times \mathbf{B}$ drift occurs to the west of the peak change in parallel drift.
153 The separation of the peak perturbation drifts ranges from 25–100 km along the east-west
154 axis. The peak density is typically is found between the two peak drifts. This structure is
155 observed in all seasons and both hemispheres; it is independent of the change in altitude
156 of the orbit track. The apex altitudes associated with the enhancements reported here
157 range from 483 km (Figure 5) to 1045 km (Figure 3). This structure was not reported
158 in previous *in situ* data. *Le et al.* [2003] shows that the peak density occurs at the same
159 longitude as the peak drifts in all three directions for ROCSAT-1 data from 1999-2000.

160 4. These features are not limited to the higher magnetic latitudes. Figure 5 shows an
161 event with all the characteristics of the density enhancements in the previous two figures,
162 but it occurs near the dip equator. This may be a region of local increased density above
163 a rising depletion as seen in simulation [*Krall et al.*, 2010].

164 5. Typically, an upward meridional drift and a westward zonal drift are associated with
165 the density enhancements. The perturbations in the $\mathbf{E} \times \mathbf{B}$ drifts are consistent with those
166 seen in the westward-tilted bubbles. A notable exception is the enhancement at 17:05:10 in
167 Figure 6, which shows a strong eastward drift in panel (d). The perturbation drifts inside
168 this enhancement are similar to those observed inside an eastward-tilted bubble [*Huang*
169 *et al.*, 2010]. Note that both the “eastward-tilted” and “westward-tilted” enhancements
170 observed in Figure 6 show the same longitudinal offset between the perpendicular and
171 parallel drifts.

5. Discussion

172 While the low inclination of the C/NOFS orbit restricts the longitudinal coverage of
173 the satellite at the magnetic latitudes where density enhancements are typically expected,
174 density enhancements are frequently encountered by C/NOFS. This is consistent with
175 the statistical studies by *Park et al.* [2008a], which show that the average magnetic
176 latitude where enhancements are found decreases as solar activity decreases. The following
177 discussion is not meant to be an exhaustive study of the qualities of density enhancements
178 during extreme solar minimum; instead it provides additional insight into the structure
179 of density enhancements not previously discussed in the published literature.

5.1. Comparison to previous observations

180 The observations from C/NOFS show a number of similarities to previous observations,
181 but are markedly different in the velocity structure across the plasma density enhance-
182 ment. As stated in the previous section, the peak change in ion drift parallel to the
183 magnetic field occurs 25–100 km to the east of the peak change in the drift perpendic-
184 ular to \mathbf{B} . To better compare these events to previous *in situ* studies of plasma density
185 enhancements, several of the plasma enhancements observed in data from ROCSAT-1 are
186 plotted in Figure 7. These particular events are discussed in greater detail in *Le et al.*
187 [2003]. The perturbation drifts associated with the enhancement all peak simultaneously
188 (*i.e.*, at the same longitude) for the events observed by ROCSAT.

189 It should be noted that ROCSAT has a larger orbital inclination than C/NOFS (35°
190 as compared to 13°). Consequently, the typical orbit of C/NOFS is nearly perpendicular
191 to the geomagnetic field lines, while the angle between a typical ROCSAT orbit and \mathbf{B} is
192 smaller ($\sim 50^\circ$ in the case of Figure 7). Despite these differences, it is not expected that

193 the ROCSAT orbit track relative to the flux tube containing the density structures would
194 mask a separation between the velocity peaks as observed in the C/NOFS data.

195 A potential source of the difference between the C/NOFS and ROCSAT observations
196 is solar activity. The C/NOFS satellite has the distinction of being launched during the
197 deepest solar minimum to occur since the dawn of the space age. The C/NOFS events
198 shown here were measured when F10.7 was less than 70 sfu, while the ROCSAT event
199 was measured when F10.7=147.9. Additionally, during 2008 the H⁺/O⁺ transition height
200 was significantly lower than predicted by the IRI model for an accurate input of F10.7,
201 indicating that the ionosphere is contracted further than expected [*Heelis et al.*, 2009].
202 Evidence of a “contracted” ionosphere is supported by the comparison between the unper-
203 turbed regions around the enhancements in Figures 3-6 and those from ROCSAT. Despite
204 the fact that the ROCSAT observations are 200 km higher in altitude, they are associ-
205 ated with ion densities nearly an order of magnitude greater than those observed with
206 C/NOFS. Figure 7 also shows a greater relative concentration of O⁺ in the unperturbed
207 background than the previous figures.

5.2. Relation between depletions and enhancements

208 The perturbation $\mathbf{E} \times \mathbf{B}$ drifts observed inside the enhancements are similar to those
209 observed in the depletions. Both types of density irregularities typically are associated
210 with an upward change in meridional drift and a westward change in the zonal drift. This
211 is consistent with previous studies that suggest that polarization electric fields within a
212 density depletion are mapped down the geomagnetic field lines, forming a density en-
213 hancement above the depleted flux tube. There is a longitudinal offset between the peak
214 parallel and $\mathbf{E} \times \mathbf{B}$ drifts in the density enhancements, while the ion drifts peak in all three

215 directions at or near the same longitude for the depletions. The existence of a longitudi-
216 nal offset is persistent in the observations and independent of changes in the orbit track
217 relative to the flux tube.

218 Simulations using the SAMI3 model have shown that a slowly growing ESF plume can
219 produce $\mathbf{E} \times \mathbf{B}$ drifts that lift density upward faster than gravity moves it downward [*Krall*
220 *et al.*, 2010]. This effect occurs in simulations for low solar activity ($F_{10.7} < 100$) or when
221 the growth of a plume is slowed by a mild trans-hemispheric wind. The slow growth
222 leads to a weak super fountain [*Huba et al.*, 2009a] with perturbation drifts inside the
223 irregularities on the order of 200 m/s. This is very similar to the C/NOFS observations,
224 but the simulations do not show the longitudinal offset between the peak parallel and
225 perpendicular drift velocities [*Krall et al.*, 2009, 2010]. The lack of this offset may be due
226 in part to unique conditions during the recent extreme solar minimum.

227 The presence of a longitudinal offset may also indicate that the physics relating deple-
228 tions and enhancements must be better understood in three spatial dimensions. Instead of
229 looking merely at a depleted flux tube, a three-dimensional structure is needed to explain
230 the asymmetric velocity structure around the density enhancement. The depletion shell
231 model described in *Kil et al.* [2009] would provide the necessary longitudinal asymmetry.
232 Alternatively, zonal wind effects may also produce the necessary structure [*Huba et al.*,
233 2009b].

6. Summary and Future Work

234 The ion drift velocities inside and around plasma density enhancements observed by
235 C/NOFS are found to have a more complicated structure than previously reported. The
236 perturbation $\mathbf{E} \times \mathbf{B}$ drifts associated with the enhancements are similar to those observed

237 within plasma depletions. However, the longitudinal separation between the peak $\mathbf{E} \times \mathbf{B}$
238 and parallel drifts is a feature previously unreported either in data or in models. It is
239 unclear whether the longitudinal offset is unique to the recent protracted solar minimum
240 or if it is a relatively common feature that has yet to be observed due to the sparse coverage
241 of *in situ* measurements of three-dimensional drifts within plasma density enhancements.
242 This uncertainty is likely to be resolved as the C/NOFS satellite continues to take data
243 during the transition back to solar maximum over the next few years.

244 The plasma density enhancements in this paper were chosen to represent general obser-
245 vations in the C/NOFS data set. A statistical study of the plasma irregularities observed
246 by C/NOFS and the relation of three-dimensional ion drifts within these features is in
247 progress. Further discussion of the three-dimensional nature of plasma depletion shells
248 and associated enhancements is needed to relate these new observations to current theory.

249 **Acknowledgments.** JHK is supported by an appointment to the NASA Postdoctoral
250 Program at Goddard Space Flight Center, administered by Oak Ridge Associated Uni-
251 versities through a contract with NASA. The authors would like to thank C. S. Huang for
252 helpful discussions regarding the electric field structure inside and around plasma density
253 depletions. The Communication/Navigation Outage Forecast System (C/NOFS) mission,
254 conceived and developed by the Air Force Research Laboratory, is sponsored and executed
255 by the USAF Space Test Program.

References

256 Aveiro, H. C., and D. L. Hysell, (2010), “Three-dimensional numerical simulation of
257 equatorial F region plasma irregularities with bottomside shear flow,” *J. Geophys. Res.*,

258 115, A11321, doi:10.1029/2010JA015602.

259 Dashora, N., and R. Pandey (2005), "Observations in equatorial anomaly region of total
260 electron content enhancements and depletions," *Ann. Geophys.*, *23*, 2449-2456.

261 de La Beaujardière, O., and the C/NOFS Definition Team (2004), "C/NOFS:
262 a mission to forecast scintillations," *J. Atmos. and Sol-Terr. Phys.*, *66*, 1573,
263 doi:10.1016/j.jastp.2004.07.030.

264 de La Beaujardière, O., J. M. Retterer, R. F. Pfaff, P. A. Roddy, C. Roth, W. J. Burke,
265 Y. J. Su, M. C. Kelley, R. R. Ilma, G. R. Wilson, L. C. Gentile, D. E. Hunton, and D.
266 L. Cooke (2009), "C/NOFS observations of deep plasma depletions at dawn," *Geophys.*
267 *Rev. Lett.*, *36*, L00C06, doi:10.1029/2009GL038884.

268 Fejer, B. G., and M. C. Kelley (1980), "Ionospheric Irregularities," *Rev. Geophys. Space*
269 *Phys.*, *18*, 401.

270 Haaser, R. A., G. D. Earle, R. A. Heelis, J. H. Klenzing, W. R. Coley, R. A. Stoneback,
271 A. G. Burrell (2010), "A study of ionospheric low latitude velocity and density irregu-
272 larity correlations during solar minimum," Abstract SA51B-1624 presented at 2010 Fall
273 Meeting, AGU, San Francisco, Calif., 13-17 Dec.

274 Heelis, R. A., and W. B. Hanson, "Measurements of thermal ion drift velocity and tem-
275 perature using planar sensors," in *Measurement Techniques in Space Plasmas (Geophys.*
276 *Monogr. Ser. vol. 102)*, edited by R. F. Pfaff, J. E. Borovsky, and D. T. Young, (AGU,
277 Washington, D. C., 1998) p. 61

278 Heelis, R. A., W. R. Coley, A. G. Burrell, M. R. Hairston, G. D. Earle, M. D. Perdue,
279 R. A. Power, L. L. Harmon, B. J. Holt, and C. R. Lippincott (2009), "Behavior of the
280 O⁺/H⁺ transition height during the extreme solar minimum of 2008," *Geophys. Res.*

- 281 *Lett.*, 36, L00C03, doi:10.1029/2009GL038652.
- 282 Huang, C.-S., O. de La Beaujardière, R. F. Pfaff, J. M. Retterer, P. A. Roddy, D. E.
283 Hunton, Y.-J. Su, S.-Y. Su, and F. J. Rich (2010), “Zonal drift of plasma particles inside
284 equatorial plasma bubbles and its relation to the zonal drift of the bubble structure,”
285 *J. Geophys. Res.*, 115 A07316, doi:10.1029/2010JA015324.
- 286 Huba, J. D., J. Krall, and G. Joyce (2009a), “Atomic and molecular ion dynamics during
287 equatorial spread F,” *Geophys. Rev. Lett.*, 36, L10106, doi:10.1029/2009GL037675.
- 288 Huba, J. D., S. L. Ossakaw, G. Joyce, J. Krall, and S. L. England (2009b), “Three-
289 dimensional equatorial spread F modeling: Zonal neutral wind effects,” *Geophys. Rev.*
290 *Lett.*, 36, L19106, doi:10.1029/2009GL040284.
- 291 Kelley, M. C. (2009), “The Earth’s Ionosphere: Plasma Physics and Electrodynamics,”
292 Academic Press, Burlington, MA, 2nd edition,
- 293 Kil, H., R. A. Heelis, L. J. Paxton, and S.-J. Oh (2009), “Formation of a plasma
294 depletion shell in the equatorial ionosphere,” *J. Geophys. Res.*, 114, A11302
295 doi:10.1029/2009JA014369.
- 296 Krall, J., J. D. Huba, and C. R. Martinis (2009), “Three-dimensional modeling
297 of equatorial spread F airglow measurements,” *Geophys. Rev. Lett.*, 36, L10103,
298 doi:10.1029/2009GL038441.
- 299 Krall, J., J. D. Huba, G. Joyce, and T. Yokoyama (2010), “Density enhance-
300 ments associated with equatorial spread F,” *Ann. Geophys.*, 28, 327-337, www.ann-
301 geophys.net/28/327/2010/.
- 302 Le, G., C.-S. Huang, R. F. Pfaff, S.-Y. Su, H.-C. Yeh, R. A. Heelis, F. J. Rich,
303 and M. Hairston (2003), “Plasma density enhancements associated with equato-

304 rial spread F: ROCSAT-1 and DMSP observations,” *J. Geophys. Res.*, *108*, 1318,
305 doi:10.1029/2002JA009592.

306 Martinis, C., J. Baumgardner, M. Mendillo, S.-Y. Su, and N. Aponte (2009), “Brightening
307 of 630.0 nm equatorial spread-F airglow depletions,” *J. Geophys. Res.*, *114*, A06318,
308 doi:10.1029/2008JA013931.

309 Oya, H., T. Takahashi, and S. Watanabe (1986), “Observations of Low Latitude Iono-
310 sphere by the Impedance Probe on Board the Hinotori Satellite,” *J. Geomag. Geoelectr.*,
311 *38*, 111-123

312 Park, J., K. W. Min, J.-J. Lee, H. Kil, V. P. Kim, H.-J. Kim, E. Lee, and D. Y. Lee (2003),
313 “Plasma blob events observed by KOMPSAT-1 and DMSP F15 in the low latitude
314 nighttime upper ionosphere,” *Geophys. Res. Lett.*, *30*, 2114, doi:10.1029/2003GL018249.

315 Park, J., K. W. Min, V. P. Kim, H. Kil, H. J. Kim, J. J. Lee, E. Lee, S. J.
316 Kim, D. Y. Lee, M. Hairston (2008), “Statistical description of low-latitude plasma
317 blobs as observed by DMSP F15 and KOMPSAT-1,” *Adv. Space Res.*, *41*, 650-654,
318 doi:10.1016/j.asr.2007.04.089.

319 Park, J., K. W. Min, V. P. Kim, H. Kil, H. J. Kim, J. J. Lee, E. Lee, S. J. Kim, D. Y.
320 Lee, M. Hairston (2008), “Magnetic signatures and conjugate features of low-latitude
321 plasma blobs as observed by the CHAMP satellite,” *J. Geophys. Res.*, *113*, A09313
322 doi:10.1016/j.asr.2008Ja013211.

323 Pfaff, R., D. Rowland, H. Freudenreich, K. Bromund, G. Le, M. Acuña, J. Klenzing,
324 C. Liebrecht, S. Martin, W. J. Burke, N. C. Maynard, D. E. Hunton, P. A. Roddy,
325 J. O. Ballenthin, and G. R. Wilson (2010), “Observations of DC Electric Fields in
326 the Low Latitude Ionosphere and Their Variations with Local Time, Longitude, and

- 327 Plasma Density during Extreme Solar Minimum,” *J. Geophys. Res.*, *115*, A12324,
328 doi:10.1029/2010JA016023.
- 329 Pimenta, A., Y. Sahai, J. A. Bittencourt, and F. J. Rich (2007), “Ionospheric plasma
330 blobs observed by OI 630 nm all-sky imaging in the Brazilian tropical sector during
331 the major geomagnetic storm of April 6-7, 2000,” *Geophys. Rev. Lett.*, *34*, L02820,
332 doi:10.1029/2006GL028529.
- 333 Watanabe, S., and H. Oya (1986), “Occurrence Characteristics of Low Latitude Iono-
334 sphere Irregularities Observed by Impedance Probe on Board the Hinotori Satellite,”
335 *J. Geomag. Geoelectr.*, *38*, 125-149.
- 336 Woodman, R. F., and C. La Hoz (1976), “Radar Observations of F Region Equatorial
337 Irregularities,” *J. Geophys. Res.*, *81*, p 5447.
- 338 Yokoyama, T., S.-Y. Su, and S. Fukao (2007), “Plasma blobs and irregularities concu-
339 rently observed by ROCSAT-1 and Equatorial Atmosphere Radar,” *J. Geophys. Res.*,
340 *112*, A05311, doi:10.1029/2006JA012044.

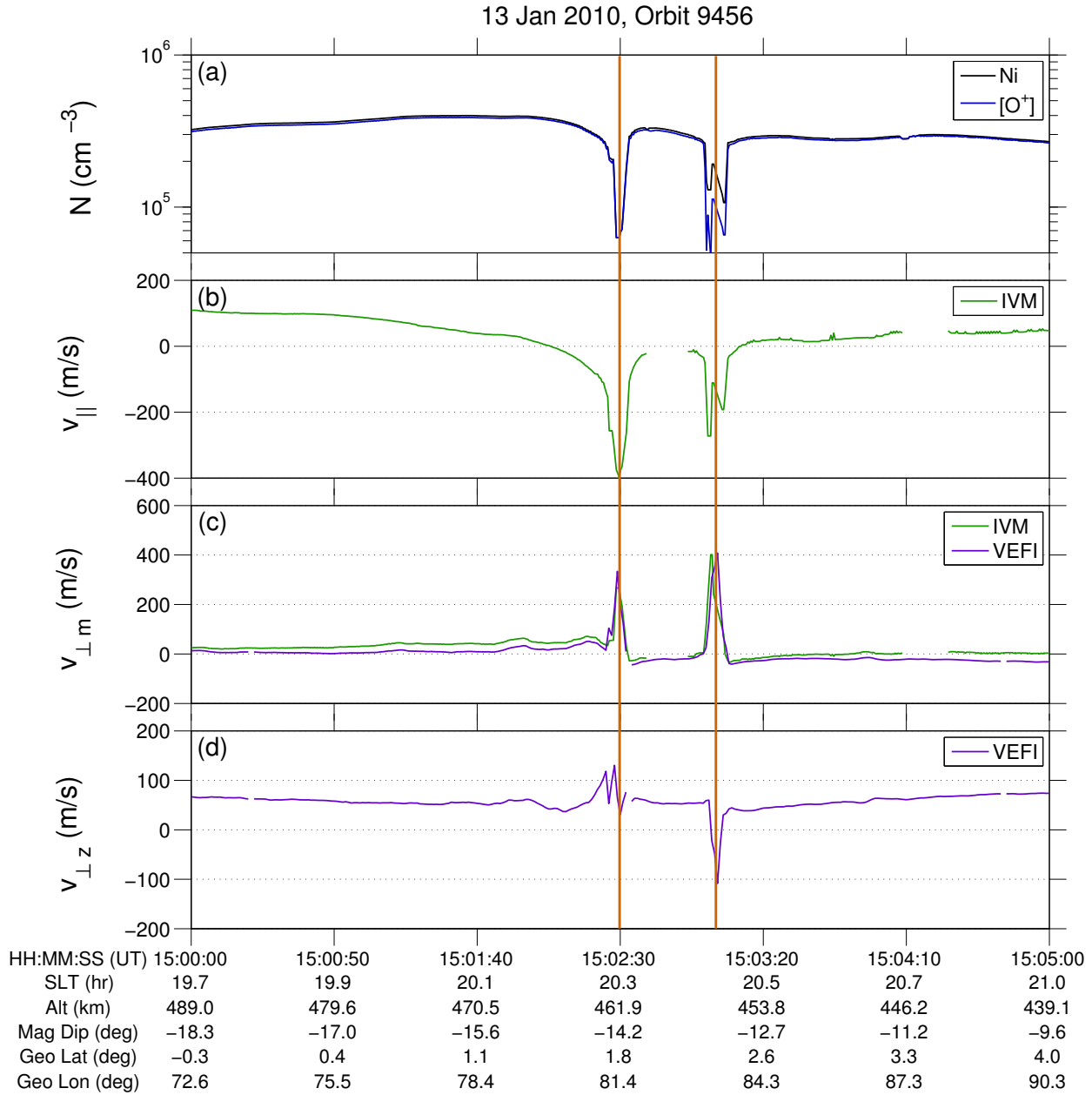


Figure 1. Plasma density depletions observed south of the magnetic dipole equator. The panels show (a) total ion density (along with the O^+ density; the remainder is H^+ and He^+), (b) ion drift parallel to the magnetic field (positive northward), (c) $\mathbf{E} \times \mathbf{B}$ meridional drift (positive upward), and (d) $\mathbf{E} \times \mathbf{B}$ zonal drift (positive eastward). The three events exhibit a clear poleward (negative) change in the parallel drift. The apex altitude for these events is 567 km.

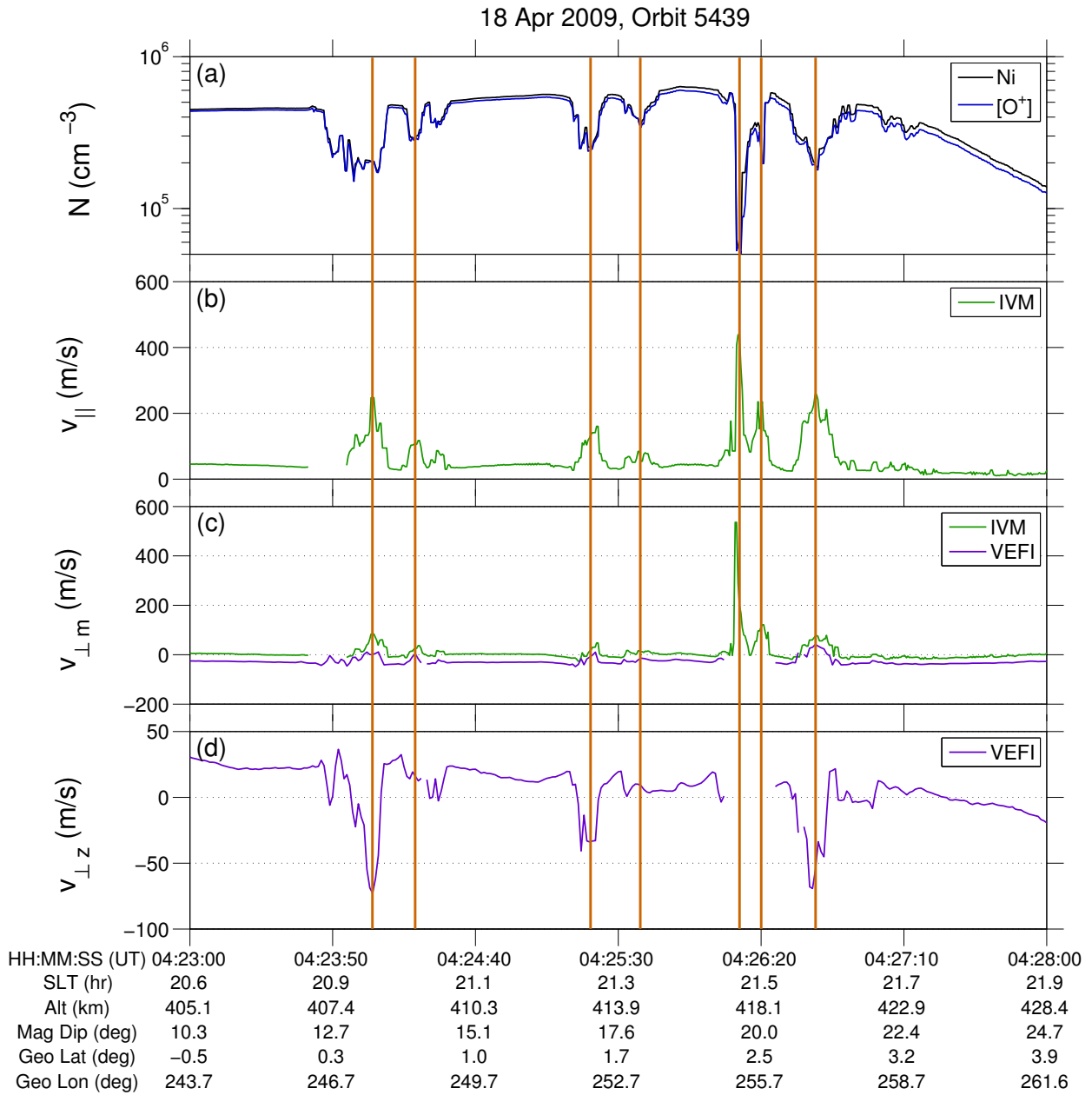


Figure 2. Plasma density depletions observed north of the magnetic dipole equator. All events exhibit a clear poleward (positive) change in the parallel drift. The format is the same as in Figure 1. The apex altitude for these events is 596 km.

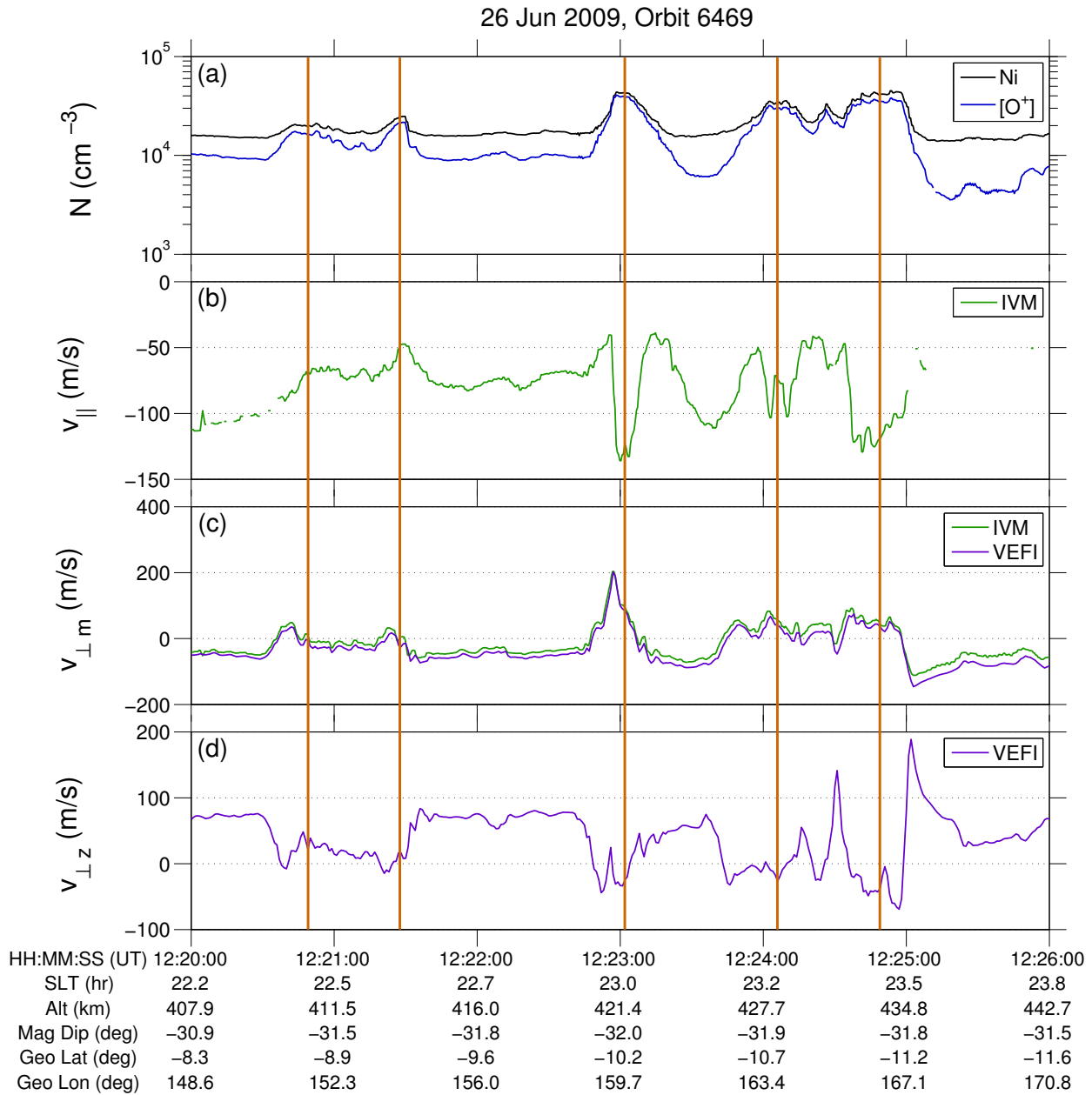


Figure 3. Plasma density enhancements observed near June Solstice 2009 in the southern magnetic hemisphere. Two of the events exhibit a clear poleward (negative) change in the parallel drift, while the two weakest density enhancements show an equatorward (positive) drift. The apex altitude for these events is 1045 km.

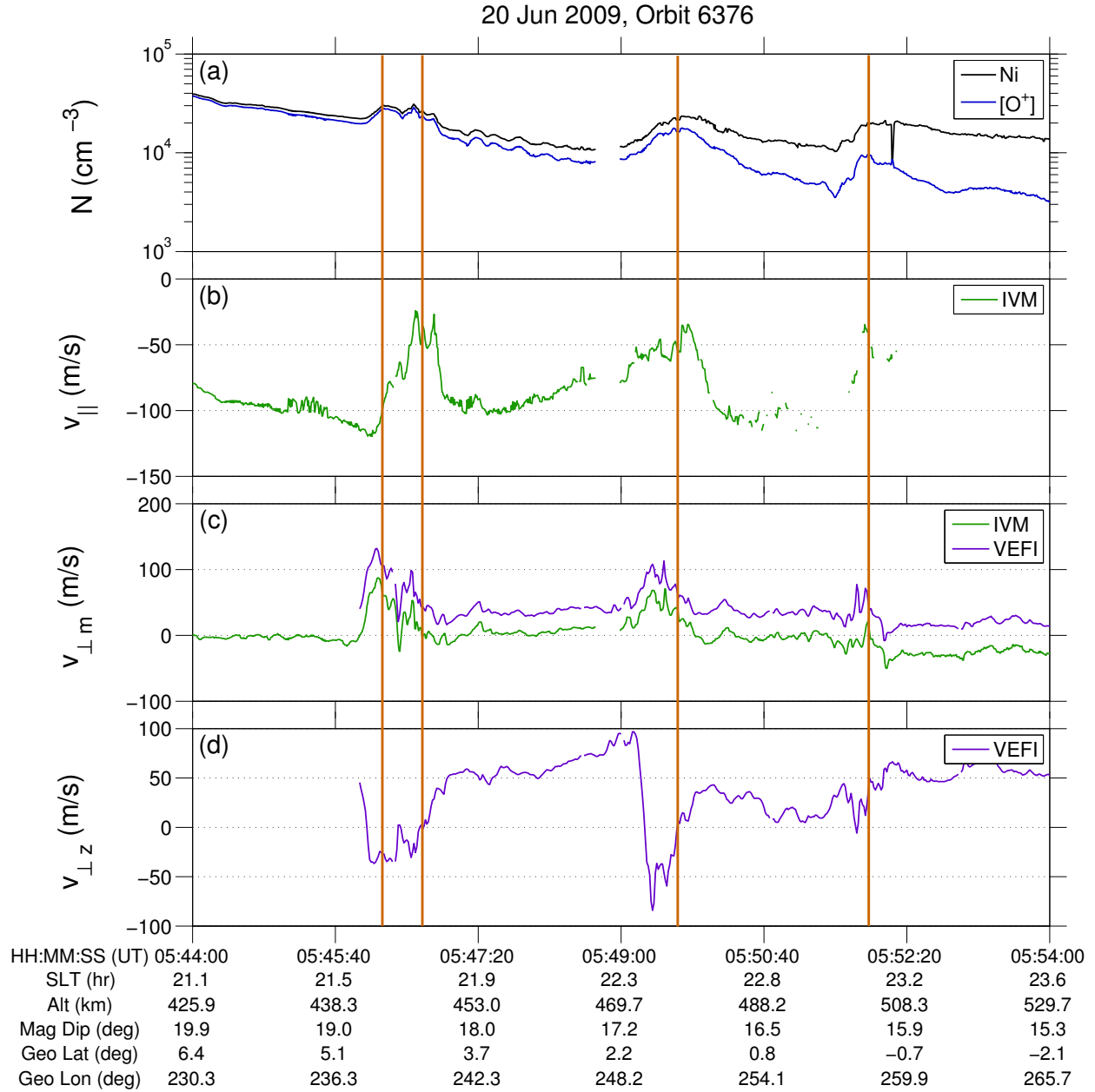


Figure 4. Plasma density enhancements observed near June solstice 2009 in the northern magnetic hemisphere. All of the events show a poleward (positive) change in parallel flow. The apex altitude for these events is 636 km.

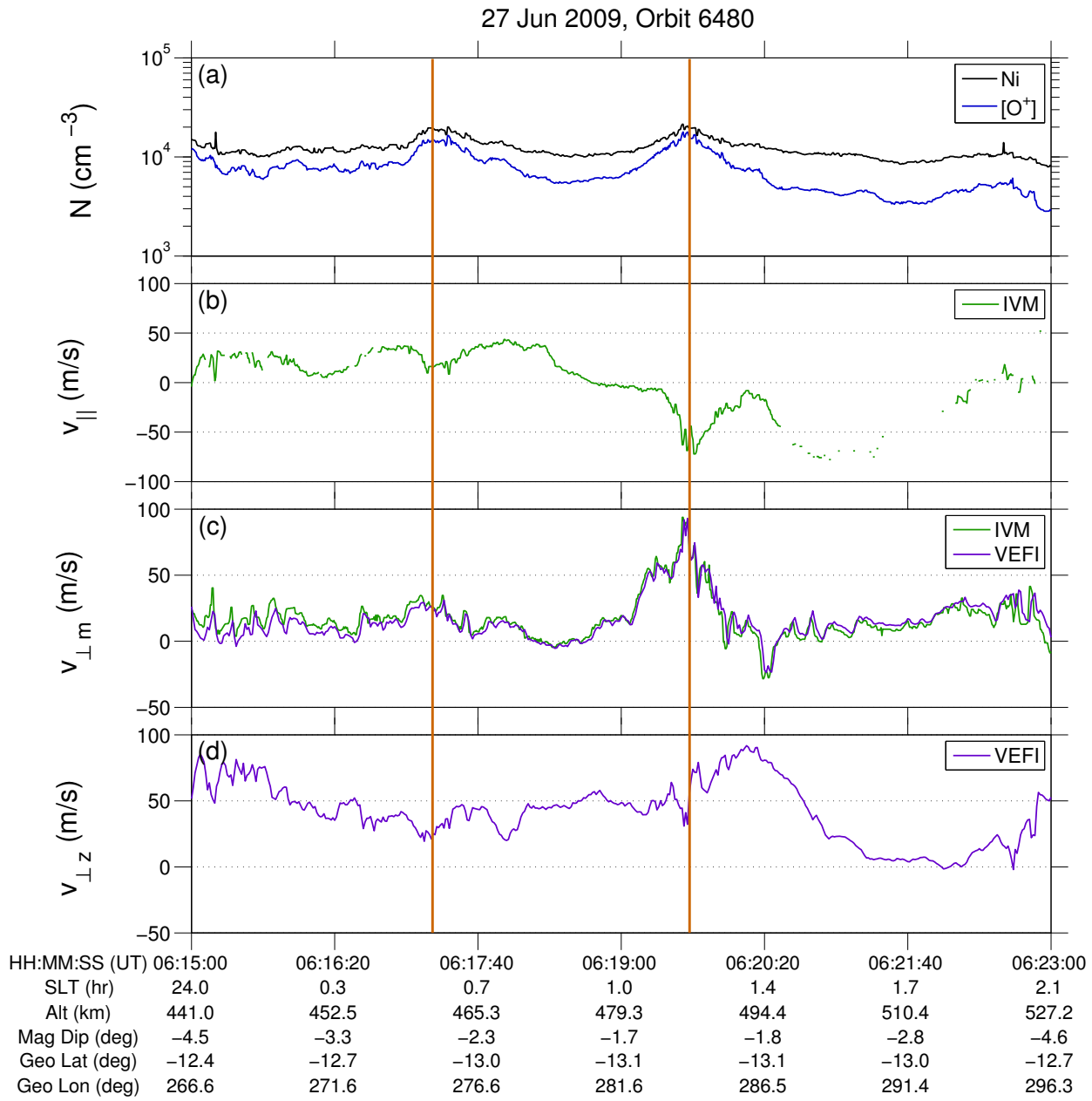


Figure 5. Plasma density enhancements observed near June Solstice 2009 near the magnetic equator. The apex altitude for these events is 483 km.

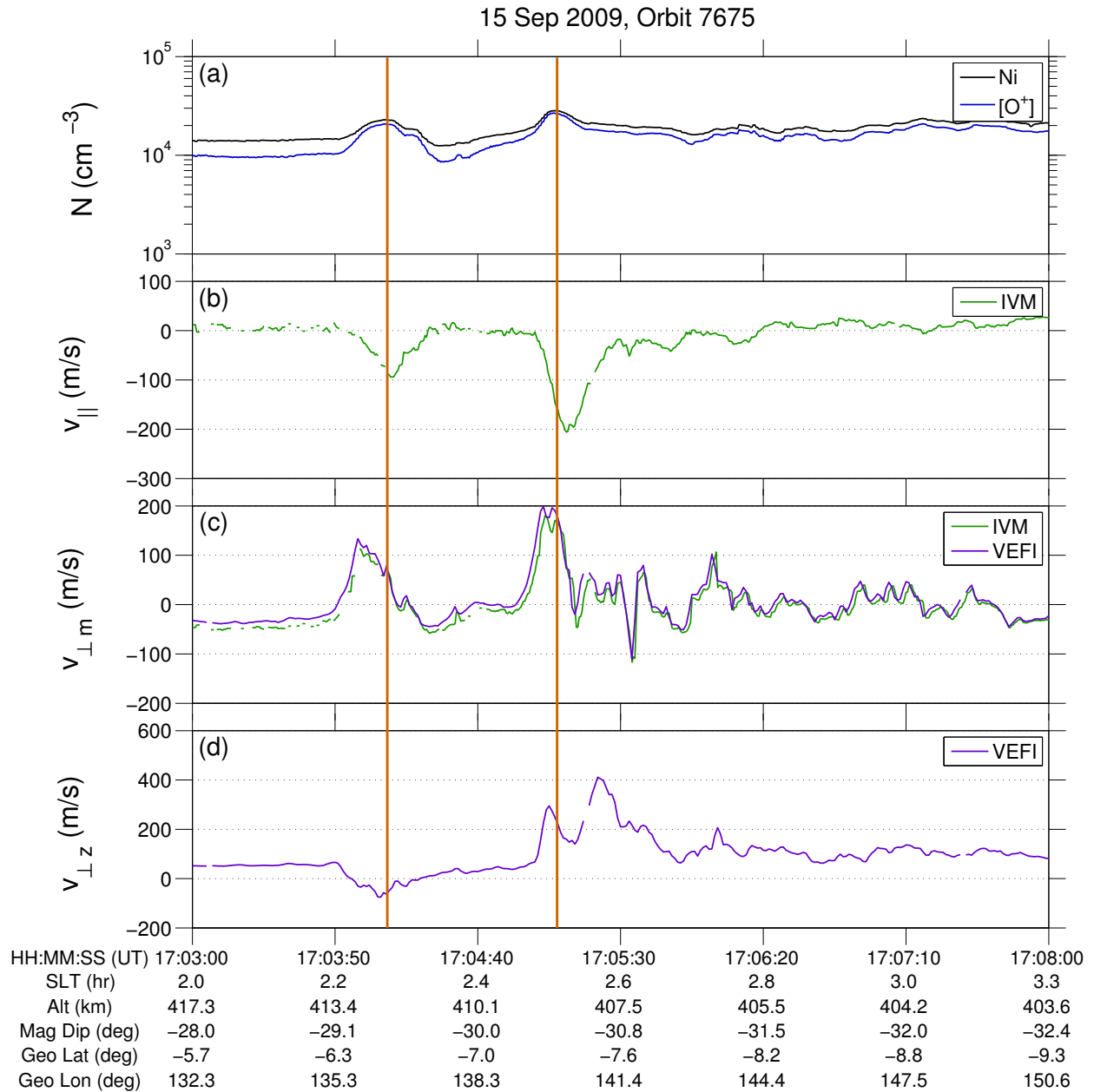


Figure 6. Plasma density enhancements observed near September Equinox 2009 in the southern magnetic hemisphere. The enhancement near 17:05:10 is associated with eastward perturbation drift. The apex altitude for these events is 974 km.

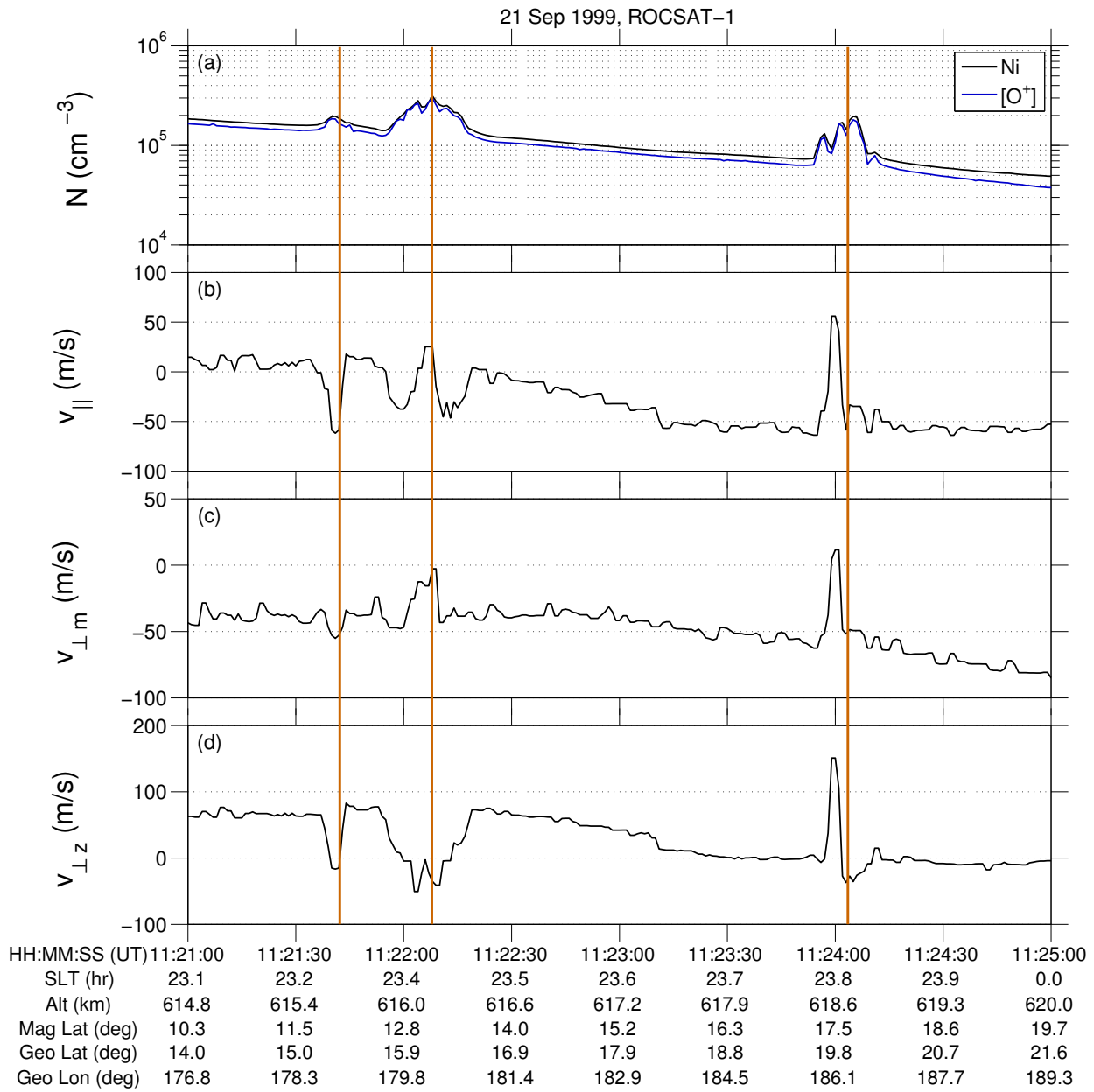


Figure 7. Plasma density enhancements observed from the ROCSAT-1 satellite. These events are discussed in detail in Le *et al.* [2003].